

Magnetic bead manipulation in a sub-microliter fluid volume applicable for biosensing

R. J. S. Derks · A. Dietzel · R. Wimberger-Friedl · M. W. J. Prins

Received: 28 April 2006 / Accepted: 4 August 2006 / Published online: 16 September 2006
© Springer-Verlag 2006

Abstract Magnetic actuation principles using superparamagnetic beads suspended in a fluid are studied in this paper. An experimental setup containing a sub-microliter fluid volume surrounded by four miniaturized electromagnets was designed and fabricated. On the basis of optical velocity measurements, the induced behavior of single beads and ordered chains was analyzed and compared to a theoretical model. This research can be used to develop new techniques for accelerated transportation in lab-on-a-chip bio-assays.

Keywords Magnetic bead manipulation · Lab-on-a-chip bio-assay · Transport acceleration · Optical velocity measurement · Bead chain formation

R. J. S. Derks (✉) · A. Dietzel
Department of Mechanical Engineering,
Micro- and NanoScale Engineering,
Eindhoven University of Technology,
PO Box 513, 5600 MB Eindhoven, The Netherlands
e-mail: r.j.s.derks@tue.nl

A. Dietzel
e-mail: a.h.dietzel@tue.nl

R. Wimberger-Friedl · M. W. J. Prins · R. J. S. Derks
Healthcare Devices and Instrumentation,
Philips Research, High Tech Campus 4,
5656 AE Eindhoven, The Netherlands
e-mail: reinhold.wimberger-friedl@philips.com

M. W. J. Prins
e-mail: menno.prins@philips.com

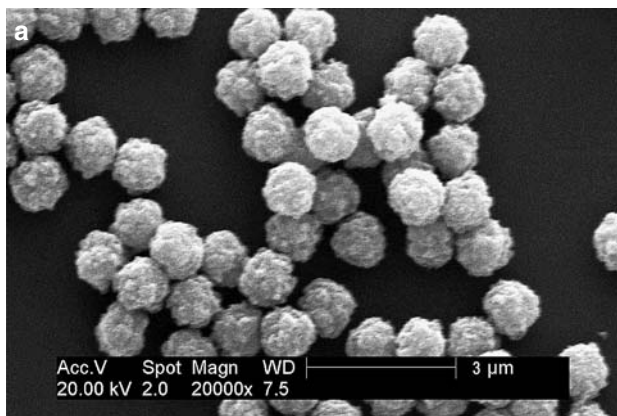
M. W. J. Prins
Department of Applied Physics,
Molecular Biosensors for Medical Diagnostics,
Eindhoven University of Technology,
PO Box 513, 5600 MB Eindhoven, The Netherlands

1 Introduction

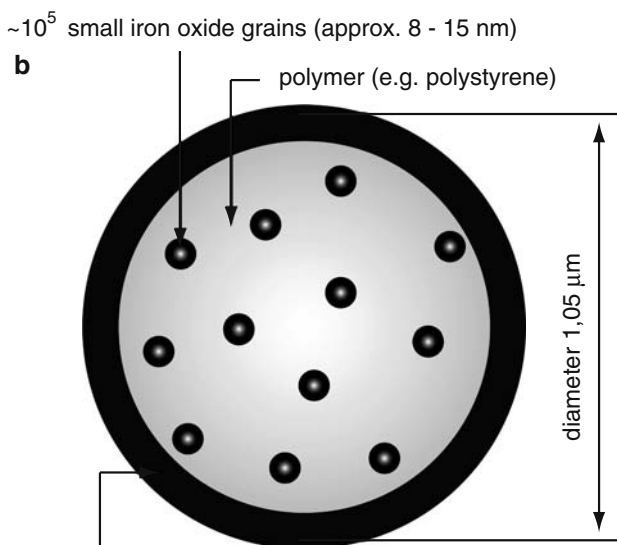
Miniaturization and integration are key aspects of future biomedical diagnostics technologies and are driven by the need for speed, reliability, sensitivity, reducing costs and to minimize human intervention (Tüdös et al. 2001). One of the challenges in miniaturized systems is to generate effective mixing and transportation, because molecular diffusion alone leads to unacceptably long reaction times. New miniaturized sensing technologies based on the usage of magnetic beads are currently under investigation in many research groups (Megens and Prins 2005; Neuberger et al. 2005). Because biological matter is barely magnetic, these techniques can be used in complex biological samples without interference. The combination of magnetic detection with magnetic bead transport seems very promising for sensitive, rapid and miniaturized bio-assays (Ottino 1990; Luxton et al. 2004; Wild 2001; Nguyen and Wu 2005; Gijs 2004).

Magnetic beads can range from tens of nanometers up to several micrometers in diameter (Fig. 1a). Generally, beads consist of many ($\sim 10^5$) separated small (8–15 nm) iron oxide grains that are embedded in a polymer matrix, for example polystyrene (Fig. 1b). This composition leads to a superparamagnetic behavior (Fig. 1c), giving a strong magnetizability in combination with a disappearance of magnetic moment after switching off the external magnetic fields (Gijs 2004; Dynal Biotech, <http://www.dynalbiotech.com>). Another important aspect is observed when the magnetic field is switched on: the beads may form chains aligned with the field lines.

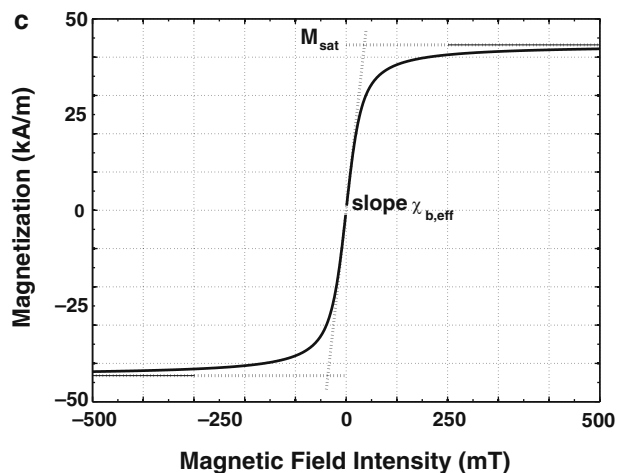
In this paper we study the motion of individual beads and chains of beads in a sub-microliter magnetic



◀ **Fig. 1** A scanning electron microscope (SEM) image of several solution dried Dynal® Dynabeads® MyOne™ Carboxylic Acid (DynaL Biotech) of 1.05 μm in diameter, which are used in the experiments (a). A single bead consists of approximately 10⁵ iron oxide grains of approximately 8–15 nm (b). These are embedded in a highly cross-linked matrix of polystyrene that is encapsulated with a hydrophilic shell of glycidyl ether with a thickness of approximately 25 nm. A vibrating sample magnetometer (VSM) measurement of a high concentrated bulk solution of these beads shows a superparamagnetic behavior (c), with a high magnetic saturation value (43.2 kA/m) and no remanent magnetization after removal of external fields (DynaL Biotech)



hydrophilic shell of glycidyl ether (approx. 25 nm)



bead manipulation device. We derive the equations of motion for single beads and chains, we describe the design and fabrication of the bead manipulator and we discuss the experimental results.

2 Equations of motion

The magnetic force \vec{F}_m acting on a single bead, approximated by a point-like magnetic dipole with a magnetic moment \vec{m}_b , is proportional to the gradient of the field \vec{B} and given by (Young and Freedman 1996; Pankhurst et al. 2003; Jackson 1998):

$$\vec{F}_m = (\vec{m}_b \cdot \nabla) \vec{B}. \tag{1}$$

The magnetic moment of a superparamagnetic bead is induced by a field $\vec{B} = \mu_0 \cdot \vec{H}$ and can be expressed as $\vec{m}_b = V_b \cdot \chi_{b,eff} \cdot \vec{H}$. Parameter V_b is the volume of the bead and $\chi_{b,eff}$ the effective magnetic susceptibility of the bead, including demagnetization effects (the demagnetization factor for a sphere is 1/3). Because the magnetic susceptibility of the surrounding medium is assumed to be zero and there are no time varying fields or currents in the medium or bead, we can adapt Eq. 1 to the case of a superparamagnetic bead as (Pankhurst et al. 2003):

$$\vec{F}_m = \frac{V_b \cdot \chi_{b,eff}}{2 \cdot \mu_0} \nabla \vec{B}^2. \tag{2}$$

A vibrating sample magnetometer (VSM) measurement has been carried out for beads suspended in fluid (Fig. 1c) (DynaL Biotech). It is clear that at higher field intensities the magnetization does not increase linearly by slope $\chi_{b,eff}$ anymore. The magnetization reaches its saturation \vec{M}_{sat} , where the magnetization is no longer dependent on the applied field. For this case, the magnetic force on a single bead is no longer given by Eq. 2 but can be expressed as:

$$\vec{F}_m = V_b \cdot \vec{M}_{sat} \cdot \nabla \vec{B}. \tag{3}$$

The magnetic attraction forces given in Eqs. 2 and 3 generate movement of a bead in a fluid, which causes a hydrodynamic drag force. For a spherical single bead

without surface roughness, the drag force can be calculated with Stokes law (Happel and Brenner 1973):

$$\vec{F}_d = -6 \cdot \pi \cdot \eta_f \cdot r_b \cdot \vec{v}_b. \tag{4}$$

The dynamic viscosity of the surrounding fluid is given by η_f . The hydrodynamic radius of the bead is assumed to be equal to the material radius r_b of the bead. The speed of the bead relative to the surrounding fluid (that is assumed to be static) is given by \vec{v}_b . Equations 2 and 4 can now be combined using the equation of motion $m \cdot \ddot{x} = F_m + F_d$. The beads are accelerated in a small negligible time ($\sim 10^{-6}$ s) to their maximum velocity. Therefore \vec{v}_b can be expressed as (Gijs 2004; Pankhurst et al. 2003):

$$\vec{v}_b = \frac{\chi_{b,\text{eff}} \cdot r_b^2}{9 \cdot \mu_0 \cdot \eta_f} \nabla \vec{B}^2. \tag{5}$$

In case of a bead in magnetic saturation, Eq. 4 has to be combined with Eq. 3, giving:

$$\vec{v}_b = \frac{2 \cdot \vec{M}_{\text{sat}} \cdot r_b^2}{9 \cdot \eta_f} \nabla \vec{B}. \tag{6}$$

These equations are only valid if the induced motion is perpendicular to gravitational forces and if Brownian motion does not play a significant role. For beads with a diameter of approximately 1 μm , Brownian motion lead to superimposed velocities in random directions below 100 nm/s and can therefore be neglected.

Magnetic beads that aggregate in chains require a different analysis due to the large transformation in shape. In a first approximation, one could assume that the total magnetic moment of a chain is given by the summation of all magnetic moments of the beads in a chain. However, dipole interactions between neighboring beads induce a change in the demagnetization fields, represented by the demagnetization factor N_d that is linked to the magnetic susceptibility by (Jackson 1998):

$$N_d = \frac{\chi_{\text{int}} - \chi_{\text{eff}}}{\chi_{\text{int}} \cdot \chi_{\text{eff}}}. \tag{7}$$

The intrinsic susceptibility χ_{int} is a material parameter and remains constant. The effective susceptibility χ_{eff} will change because of the change in demagnetization.

We performed numerical simulations in Comsol Multiphysics (<http://www.comsol.com>) to study the influence of the chain shape on the demagnetization

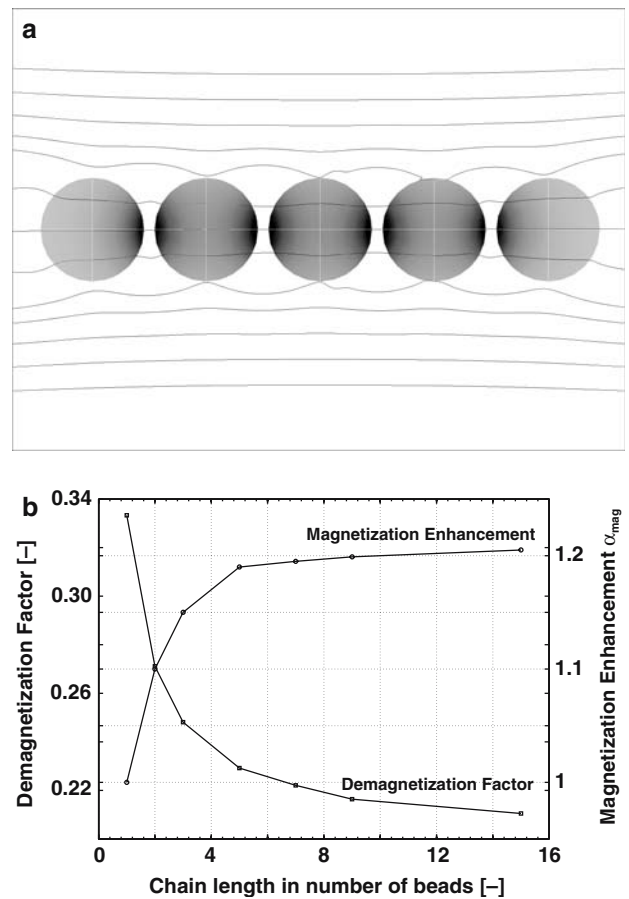


Fig. 2 A Comsol Multiphysics model is created to investigate the magnetization enhancement by chain formation of beads (a). A homogenous magnetic field intensity of 15 mT is applied on the beads ($\chi_{b,\text{eff}} = 1.52$) with a diameter of 1 μm that are spaced from each other by twice the shell thickness (2×25 nm). The magnetic field lines concentrate in the chain, creating a higher magnetization on the points of contact. The demagnetization factor is decreased by the increasing number of beads in the chain, and the average bead magnetization is increased to a maximum enhancement of 1.2, practically already reached at a chain length of 5 beads (b)

factor and the resulting magnetization (Fig. 2a). The chain is modeled as a row of spheres each of 1 μm in diameter and with the same intrinsic susceptibility as the single beads. The spacing of 50 nm represents twice the non-magnetic shell of the beads (Fig. 1b). The simulations show that the demagnetization factor is reduced by increasing the number of beads in the chain. We defined a magnetization enhancement as $\alpha_{\text{mag}} = \chi_{c,\text{eff}}/\chi_{b,\text{eff}}$, where $\chi_{c,\text{eff}}$ is the effective susceptibility of a chain. This magnetization enhancement approaches a maximum already in the case of five beads in a chain (Fig. 2b). By defining the chain length as l_c and using the already defined bead radius r_b , the number of beads can be given by $n = l_c/(2 \cdot r_b)$. The

magnetic force on a long chain can now be expressed as:

$$\vec{F}_m = \frac{\pi \cdot l_c \cdot r_b^2 \cdot \alpha_{\text{mag}} \cdot \chi_{b,\text{eff}}}{3 \cdot \mu_0} \nabla \vec{B}^2. \quad (8)$$

The hydrodynamic resistance on a chain also highly depends on its shape and orientation. The hydrodynamic resistance of elongated bodies, axially dragged in a viscous fluid can be approximated as follows (Happel and Brenner 1973):

$$\vec{F}_d = \frac{C_1 \cdot \pi \cdot \eta_f \cdot 1/2l_c}{\ln(l_c/r_b) + C_2} \cdot \vec{v}_c. \quad (9)$$

In this approximation, C_1 and C_2 are dimensionless constants that describe the hydrodynamic shape of the body, which have to be determined experimentally. If we now combine Eqs. 8 and 9, the velocity of a chain relative to the medium can be derived:

$$\begin{aligned} \vec{v}_c &= \left(\frac{(\ln(l_c/r_b) + C_2) \cdot \alpha_{\text{mag}}}{1/6 \cdot C_1} \right) \cdot \left(\frac{r_b^2 \cdot \chi_{b,\text{eff}}}{9 \cdot \mu_0 \cdot \eta_f} \nabla \vec{B}^2 \right) \\ &= \left(\frac{(\ln(l_c/r_b) + C_2) \cdot \alpha_{\text{mag}}}{1/6 \cdot C_1} \right) \cdot \vec{v}_b. \end{aligned} \quad (10)$$

The above equation shows that the chain velocity \vec{v}_c is proportional to the velocity of a single bead \vec{v}_b . The proportionality—or in this case enhancement—factor that is shown in brackets on the right in Eq. 10, depends on the aspect ratio l_c/r_b , the hydrodynamic constants C_1 and C_2 and the magnetic enhancement factor α_{mag} , but not on the magnetic field.

3 The magnetic bead manipulator

To investigate the bead and chain behavior induced by external magnetic fields, an experimental setup was designed and fabricated (Fig. 3). This magnetic bead manipulator consists of a fluid container, surrounded by four miniaturized solenoids to generate a wide variety of magnetic field shapes.

Because future miniaturized biosensor applications will generally consume sub-microliter volumes, the magnetic bead manipulator has a cylindrical fluid volume with a diameter of 1 mm and a depth of 200 μm . The beads are observed with an optical microscope that is able to resolve beads with a diameter down to 300 nm. The working distance of the microscope limits the outer diameter of the solenoids. Soft iron cores

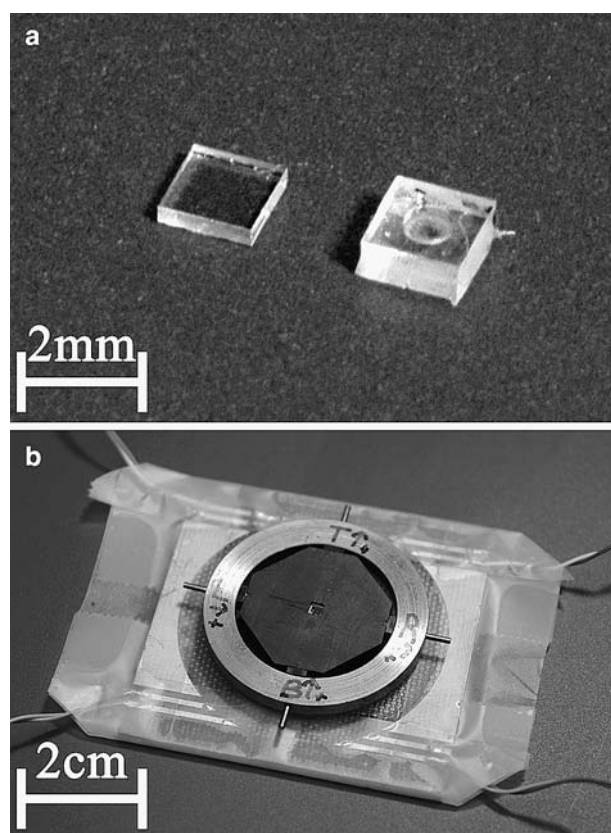


Fig. 3 The design of the magnetic bead manipulator contains a sub-microliter fluid volume that is surrounded by four miniaturized solenoids, capable to create a large variety of magnetic field shapes. The fluid containers with dimensions of 2 mm \times 2 mm are fabricated out of polydimethylsiloxane (PDMS) by molding and are closed with glass cover sheets of 400 μm thick, sawed in the same lateral dimensions as the containers (a). The other components of the magnetic bead manipulator are fabricated with conventional techniques. The magnetic field intensity is increased by the usage of cores and a surrounding yoke that guide the flux lines. From the top, a microscope is used to observe the bead manipulation in the fluid volume, which is able to resolve beads with a diameter down to 300 nm. The black aluminium casing is used to assemble all components in the right position. After assembly, the device is mounted on a PCB board to create solid electrical connection points and to facilitate the placement under the microscope (b)

are inserted in the solenoids and are coupled with a surrounding yoke to minimize air gaps and to increase the field intensity in the fluid volume. To suppress the influence of flaring field lines, the inner diameter of the solenoids is larger than the fluid volume diameter.

The four solenoids with an inner diameter of 1 mm, an outer diameter of 2.5 mm, a length of 5 mm and 294 windings were constructed using a \varnothing 100 μm bonding wire. The cores and surrounding yoke are machined out of soft-iron to minimize remanent magnetic fields. A casing to assemble all components in the exact position is machined out of aluminium with a very low

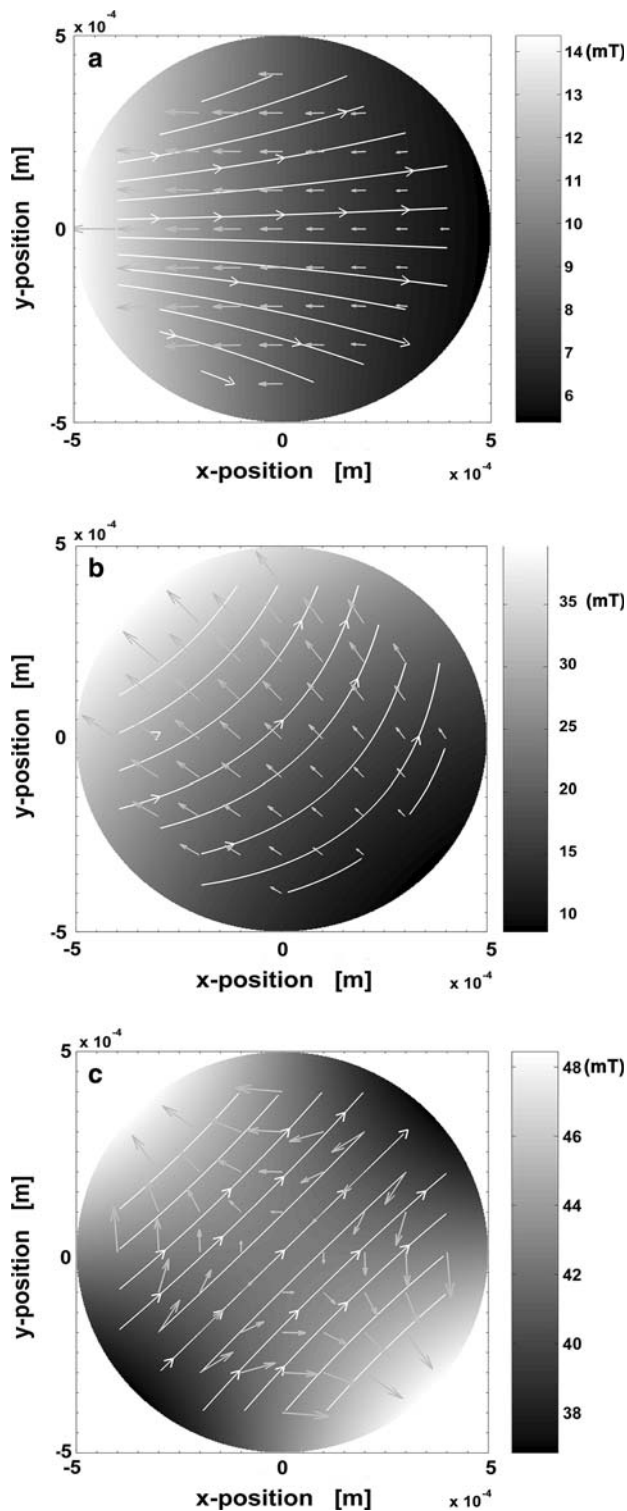


Fig. 4 Magnetic field simulations are carried out in Comsol Multiphysics to investigate the performance and flexibility of the magnetic bead manipulator. For the experiments, one solenoid is powered with a current of 75 mA, generating magnetic field intensities of 15 mT (to preserve the magnetic susceptibility to be constant) that results in expected velocities of 5 $\mu\text{m/s}$ at maximum for beads with a diameter of 1.05 μm and a susceptibility $\chi_{b,\text{eff}} = 1.52$ (a). When two solenoids are both powered with a high current of 130 mA, a unilateral velocity vector field is created that can be rotated in any direction, with velocities of approximately 20 $\mu\text{m/s}$ (b). Applying this current on the four solenoids at the same time, a magnetic field with a maximum of 48.5 mT is generated that creates a complex bead velocity vector field with maximum bead velocities of approximately 40 $\mu\text{m/s}$ (c). In all simulations, a value of $2.1 \times 10^{-3} \text{ kg/m s}$ is used for the viscosity η of the density matched fluid

wafer that consists of an array of circular posts. A pre-mixture of a silicone elastomer (Sylgard 184 base) and a curing agent elastomer (Dow Corning) is poured over the whole wafer and placed in a sandwich curing plate equipped with three adjustable micro-meter screws to set the final height of the containers.

After curing, the PDMS slice is torn off the wafer and laser-cut into individual containers with outer dimensions of 2 mm \times 2 mm. Bovine serum albumin (BSA) is applied on all walls of the fluid container to increase the hydrophilicity of the PDMS surface (originally highly hydrophobic). To close the containers, glass cover sheets are used that were sawed into the same lateral dimensions.

The complete magnetic bead manipulator is mounted on a PCB board to facilitate the handling and to create solid electrical connection points (Fig. 3b). The magnetic bead manipulator is placed under a microscope (objective M = 65, NA = 0.70, WD = 1.30 mm) equipped with a digital camera (resolution 720 \times 576 pixels, frame rate 25 fps), connected to a DVD recorder. A four-channel home-built current source ($I_{\text{max}} = 250 \text{ mA}$ over $R = 3 \Omega$) is used to power the solenoids separately. With use of a D/A converter, the current source is controlled with scripts that are written in Matlab. A height gauge is mounted just below the microscope base-plate to control the position of the view plane in the fluid volume.

Numerical simulations were carried out in Comsol Multiphysics (<http://www.comsol.com>) in order to investigate a variety of magnetic fields induced by the electromagnets. In the first simulation, one solenoid is powered with a low current of 75 mA (Fig. 4a). The maximum magnetic field intensity is 15 mT at the border of the fluid volume, as illustrated by the color map (gray scale). The bead trajectories are calculated with use of Eq. 5 and 6 and illustrated by the arrows. In this model, a maximum velocity of 5 $\mu\text{m/s}$ is calculated

magnetic permeability to minimize the influence on the magnetic fields.

The disposable fluid containers are fabricated out of polydimethylsiloxane (PDMS) (Fig. 3a). By photolithography and subsequent wet etching steps, an inversely shaped mold has been created on a silicon

for beads with a diameter of $1\ \mu\text{m}$. In a second simulation, the left and top solenoids are both powered by a high current of 130 mA (Fig. 4b), generating 39.7 mT at maximum. Two neighboring solenoids can be used this way to interpolate the field characteristics between the directions of the solenoids, preserving a bead velocity of $20\ \mu\text{m/s}$. In the third simulation, every solenoid is powered by a high current of 130 mA (Fig. 4c), generating maximum magnetic field intensities of 48.5 mT. The bead trajectories show a large variation, with maximum velocities of $40\ \mu\text{m/s}$. Many more (complex) field variations have been found by similar simulations, which demonstrate the high performance and flexibility of the magnetic bead manipulator.

4 Experiments

Experiments were carried out to verify the travel velocities of single beads and chains as expected by Eqs. 5 and 10, using the magnetic field prediction from the simulations (Fig. 4a). By applying the current of 75 mA through the left solenoid, single beads and chains are attracted towards the solenoid. Beads with a diameter of $1\ \mu\text{m}$ were used, commercially available from Dynal (Dynal Biotech). Their magnetic saturation occurs at much higher field intensities than reached in these experiments and therefore the magnetic susceptibility ($\chi_{b,\text{eff}} = 1.52$) can be assumed to be constant (Fig. 1c).

The stock solution of beads was diluted with water into two different concentrations. A low concentration of $200\ \mu\text{g/ml}$ ($\approx 2 \cdot 10^8$ beads/ml) minimizes chain formation, suitable to study the travel of single beads. A higher concentration of $500\ \mu\text{g/ml}$ ($\approx 5 \cdot 10^8$ beads/ml) forces the beads to aggregate in chains under the application of a magnetic field, which is used in the study on chains. By adding the inorganic salt sodium polytungstate (SPT), the bead solution was tuned to have a matching density as the beads itself ($\rho = 1.8\ \text{g/cm}^3$). This avoids out-of-plane traveling of the beads, to enable a complete bead tracking in the whole imaging plane of the microscope. SPT does not affect the neutral properties of the fluid, but increases the viscosity η to a value of $2.1 \cdot 10^{-3}\ \text{kg/m s}$, lowering the expected experimental velocities (already taken into account in the simulations).

The path of every single bead or chain was tracked from a recorded movie, using home developed processing software that is written in Matlab (Fig. 5). Every movie frame is averaged with the 25 surrounding frames to suppress background noise and subsequently

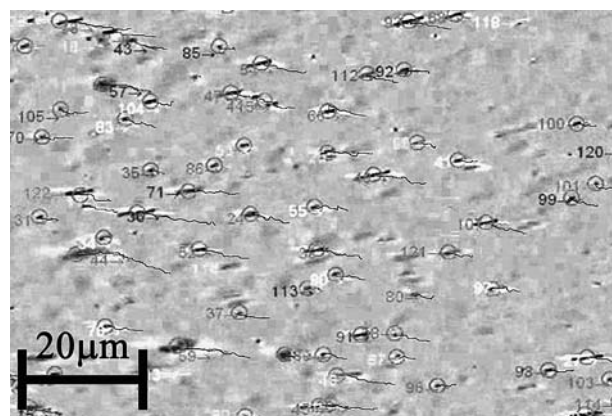


Fig. 5 The movement of beads is recorded with a digital camera that is installed on top of the microscope. Movie processing software is written for contrast enhancement and to average out background noise. The position of each individual bead or chain in every frame is obtained by finding groups of intensity peaks, and the number of beads in a chain is calculated out of the covered area. A sub-pixel resolution position is obtained by a center of mass calculation. These positions are used to plot trajectory lines for every bead or chain in the movie

all intensity peaks in the frame are identified. Neighboring intensity peaks are joined to one area and divided by the actual area of a single bead, giving the number of beads in the chain or identifying a single bead. The bead or chain position is determined with sub-pixel resolution by an estimation of the center of mass.

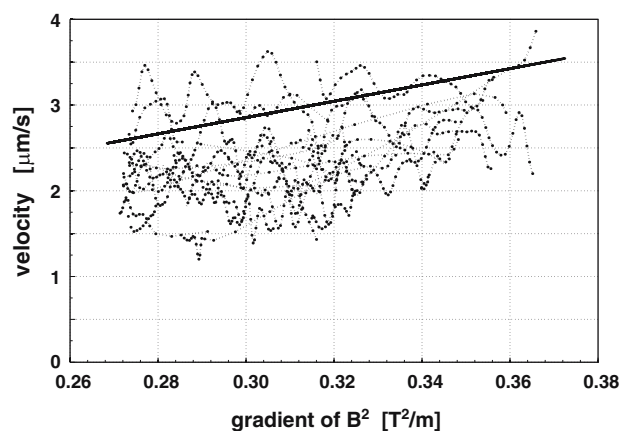


Fig. 6 The measured velocities of the single beads as a function of calculated values for ∇B^2 show a large coefficient of variation (CV) of 0.22, which could be explained by bead-to-bead variations possibly caused by the average magnetic susceptibility determined with VSM measurements. The experimental data (dotted curves) is on average noticeably lower (with an average relative error (RE) of 0.33) than the velocity predicted with Eq. 5, plotted as the solid line. This difference can be caused by (static) uncertainties in the fluid viscosity, the generated magnetic field and the bulk properties of the beads

To exclude chains that do not move in an axial direction, the relative alignment with the direction of movement is determined, which was not allowed to exceed a difference of 5 degrees. The obtained tracks are visualized in the movie as trajectory lines.

In a first experiment, the travel of single beads has been studied. For each single bead position located with the movie processing software, the actual velocity is calculated. We have plotted the experimental velocities as function of the calculated values of $\nabla \vec{B}^2$ (Fig. 6). The measured velocities are on average noticeable lower than predicted by Eq. 5, quantified by an average relative error (RE) of 0.33. Furthermore, the measurements show a large spread that is expressed as a coefficient of variation (CV) of 0.22. This RE and CV can be caused by uncertainties in the following parameters (in brackets the form in Eq. 5 is given):

- The radius and hydrodynamics of the bead including shape and surface roughness (r_b^2);
- The viscosity of the surrounding fluid ($1/\eta_f$);
- The magnetic susceptibility of the beads ($\chi_{b,eff}$);
- The magnetic field characteristics ($\nabla \vec{B}^2$);
- (computational) errors in the velocity measurement itself (\vec{v}_b).

Light scattering experiments show a small distribution in bead diameter (Dynal Biotech), affecting the experimental velocities with 20% at maximum that could contribute to the CV. The viscosity of the surrounding fluid has been increased by the density matching process. Measurements determined the fluid viscosity with an uncertainty of 5%. However, a small increase of the fluid temperature by heat dissipation of the solenoids and the illumination could lower the viscosity existential. The viscosity is therefore estimated to affect the resulting velocities at most with 20%, which could contribute to the RE. The average magnetic susceptibility per bead has been estimated by a VSM measurement in a concentrated volume of magnetic beads (Dynal Biotech). Magnetic interactions between beads in the suspension may occur during this measurement. The obtained value may therefore not reflect the single bead magnetic susceptibility (Häfeli et al. 2005; van Ommering et al. 2006), which could contribute to the RE. The measurement also conceals a contribution to the CV that could exist because of a possible but unknown variation in the iron oxide content (Häfeli et al. 2005).

The estimation of the magnetic field characteristics is based on simulations. Deviation could occur by magnetic saturation of the cores and surrounding yoke.

Simulations predicted maximum field intensities of approximately 100 mT in the flux guides (applying the same parameter values as in the experiment), which is far below the saturation level of the core and yoke material. In this point in time, we approximate the deviation in the experimental velocities because of the field characteristics to be 15% (contributing to the RE and CV), but this assumption should be validated with a magnetic field calibration. The velocity measurement and numerical calculations could also be subject of experimental error. A deviation of 10% on the

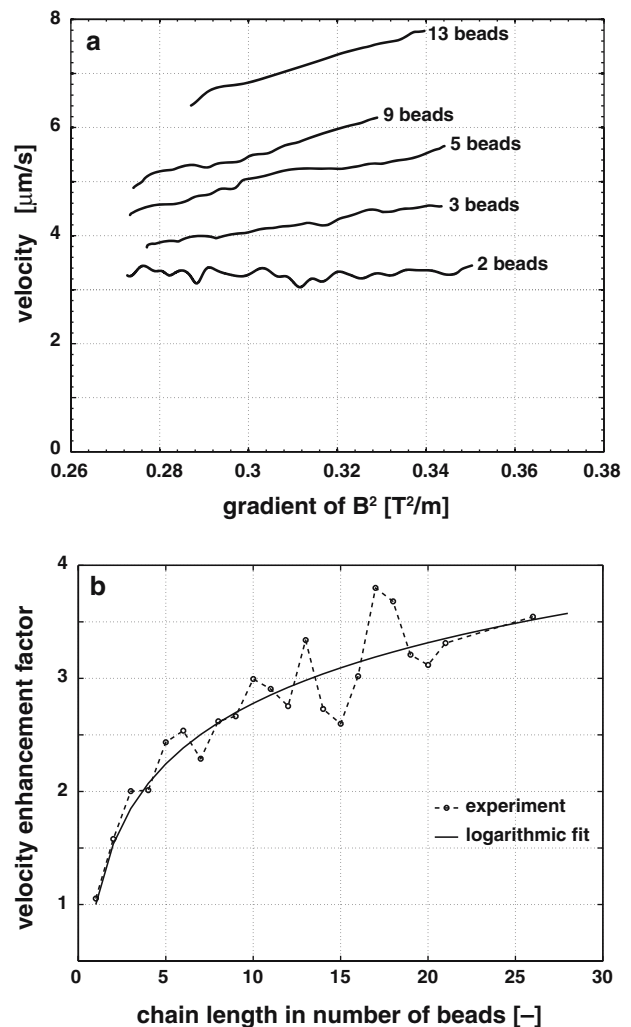


Fig. 7 The dynamics of chains are studied by gathering all trajectories of chains that have an equal length (typically 25–50 trajectories). For each chain length, the running average is calculated and plotted as a function of $\nabla \vec{B}^2$. The experiments show an increase in velocity as a function of the number of beads in the chain (a). This experimental data can be represented as a velocity enhancement factor that is a logarithmic function of the number of beads in a chain (b). The obtained function is in agreement with the enhancement factor we found in Eq. 10

experimental velocities is estimated, contributing to both the RE and CV. Considering the many potential sources of deviation, the single bead experiments were in good agreement with the established equations of motion.

The following experiment has investigated the utility of chain formation for the acceleration of transport. Because chains will align with the field lines, an axial movement of the chains can be expected, according to the simulations (Fig. 4a). For all obtained trajectory lines, the resulting velocities as a function of ∇B^2 are calculated (Fig. 7a). The shape of these curves is comparable with the curve of the single bead experiments (roughly linear). Quantitatively, we observe for the velocity of each chain length an enhancement factor normalized to the velocity of a single bead: $VEF = \bar{v}_c / \bar{v}_b$. This velocity enhancement factor depends in a logarithmic way only on the number of beads in the chain (n), approximated by (Fig. 7b):

$$VEF = 1 + 0.77 \cdot \ln(n). \quad (11)$$

The obtained function is in agreement with the velocity enhancement factor we found in Eq. 10. Using $\alpha_{\text{mag}} = 1.2$, we find a corresponding fit with $C_1 \approx 9$ and $C_2 \approx 0.56$. A comparison with values for an ordinary cylinder dragged in an axial direction through the fluid ($C_1 = 4$ and $C_2 = -0.72$) (Happel and Brenner 1973) indicates that the hydrodynamic drag force of a chain of beads is evidently higher. The undefined surface roughness and the undulating shape of the chain of beads is most likely the main reason for the higher hydrodynamic drag force.

5 Conclusions and outlook

We performed studies on the dynamics of single magnetic beads and chains of beads inside a sub-microliter device with four surrounding miniaturized electromagnets. Experiments on single beads showed velocities that can differ with a coefficient of variation (CV) of 0.22, most probably by bead-to-bead variations. The average measured velocity deviates from theoretical predictions with an average relative error (RE) of 0.33. One hypothesis is that this deviation is partially caused by the use of a susceptibility value from bulk VSM measurements, which may not reflect the actual average susceptibility of individual beads. Further experiments should be carried out to get a good overall understanding of single bead properties. Furthermore, the magnetic field in the fluid volume generated by the bead manipulator should be measured as function of its

position and compared to the simulations to confirm the accuracy of this parameter.

Equations for the influence of chain formation on the magnetization and the hydrodynamic drag force have been established and compared to experimental data. We observe a logarithmic dependence of velocity on the chain length. For a given magnetic field, the velocity of chains is proportional to the velocity of single beads with an enhancement factor that depends on the number of beads in the chain and the hydrodynamic properties of the chain.

Our experiments show that chain formation can in principle be used for accelerated transport in fluids. We envisage that the controlled rapid manipulation of chains can be beneficial for bio-assays, for example when target molecules are to be bound to magnetic particles or when enhanced mixing or transport is required. Next steps will involve the study of chain manipulation in dynamic fields, for example to generate a rotational motion of the chains. The application of bead manipulation should in further research be confirmed in biological samples.

Acknowledgments The authors would like to thank Erik Homburg for his assistance on the simulations and electronics, Kim van Ommering for her great input in developing the movie processing software, and Frans van Gaal for the realization of the experimental setup.

References

- Comsol Multiphysics, Comsol 3.2.0.222, Comsol AB. <http://www.comsol.com>
- Dynal Biotech ASA, Norway. <http://www.dynalbiotech.com>
- Gijs M (2004) Magnetic bead handling on-chip: new opportunities for analytical applications. *Microfluid Nanofluid J* 1:22–40
- Häfeli U, Lobedann M, Steingroewer J, Moore L, Riffle J (2005) Optical method for measurement of magnetophoretic mobility of individual magnetic microspheres in defined magnetic field. *J Magn Magn Mater* 293:224–239
- Happel J, Brenner H (1973) *Low Reynolds number hydrodynamics, with special applications to particulate media*. Noordhoff International Publishing, Gronigen. ISBN 9-001-37115-9
- Jackson J (1998) *Classical electrodynamics*, 3rd edn. Wiley, New York. ISBN 0-471-30932
- Luxton R, Badesha J, Kiely J, Hawkins P (2004) Use of external magnetic fields to reduce reaction times in an immunoassay using micrometer-sized paramagnetic particles as labels (magnetoimmunoassay). *Anal Chem* 76:1715–1719
- Megens M, Prins M (2005) Magnetic biochips: a new option for sensitive diagnostics. *J Magn Magn Mater* 293:702–708
- Neuberger T, Schöpf B, Hofmann H, Hofmann M, von Rechenberg B (2005) Superparamagnetic nanoparticles for biomedical applications: possibilities and limitations of a new drug delivery system. *J Magn Magn Mater* 293:483–496
- Nguyen N, Wu Z (2005) Wu micromixers—a review. *J Micro-mech Microeng* 15:1–16

- van Ommerring K, Nieuwenhuis J, van IJzendoorn L, Koopmans B, Prins M (2006) Confined Brownian motion of individual magnetic nanoparticles on a chip—characterization of magnetic susceptibility. *Appl Phys Lett* (in press)
- Ottino J (1990) *The kinematics of mixing: stretching, chaos and transport*. Cambridge University Press, Cambridge. ISBN 0-521-36335-7
- Pankhurst Q, Connolly J, Jones S, Dobson J (2003) Applications of magnetic nanoparticles in biomedicine. *J Phys D Appl Phys* 36:167–181
- Tüdös A, Besselink G, Schasfoort R (2001) Trends in miniaturized total analysis systems for point-of-care testing in clinical chemistry. *Lab Chip* 1:83–95
- Wild D (2001) *The immunoassay handbook*, 2nd edn. Nature Publishing Group, London. ISBN 0-333-72306-6
- Young H, Freedman R (1996) *University physics*, 9th edn. Addison-Wesley Publishing Company, Reading. ISBN 0-201-31132-1